Reaction Chemistry & Engineering

ROYAL SOCIETY OF CHEMISTRY

PAPER

View Article Online
View Journal | View Issue

Cite this: *React. Chem. Eng.*, 2024, 9, 2149

Extraction of the intrinsic rate constant for a photocyclization reaction in capillary microreactors using a simplified reactor model†

Jun Li, ‡*[a] Helena Šimek Tosino, ‡[b] Bradley P. Ladewig, [c] Nicole Jung,[bd] Stefan Bräse[bd] and Roland Dittmeyer [a]

Received 16th February 2024,
Accepted 9th May 2024

DOI: 10.1039/d4re00087k

rsc.li/reaction-engineering

In this work, a simple reactor model for evaluating the intrinsic rate constant of a photocyclization reaction is presented. The photoreaction was performed in a standardized capillary microreactor that ensures isothermal and uniform irradiation conditions. The effects of residence time and incident light intensity on the reaction performance were studied, and a reaction kinetic model was established based on a plug flow assumption. The reaction order with respect to the F-tagged amide precursor was found to be 2 in the photochemical transformation, and apparent rate constants under various light intensities were obtained. Comprehensive mass transport diagnostics were performed by using dimensionless numbers based on the established effective reaction kinetics. The intrinsic rate constant of the photoreaction was extracted from the experimental data using a simplified reactor model, in which a parameter representing the photon absorption fraction of the photocatalyst was introduced. Moreover, the proposed reactor model gives a general overview for improving the space–time yield of photochemical processes in microreactors.

Introduction

The indole core is one of the most widely distributed heterocycles in nature, present in the structures of many natural products, biologically active compounds, and pharmaceuticals.[1,2] Its derivatives express diverse benefits such as anticancer, antifungal, antimicrobial and anti-inflammatory activity and are important building blocks for the preparation of other related heterocycles. Conventional procedures for the indole syntheses often involve harsh reaction conditions and suffer from side reactions, producing substantial amounts of waste.[3,4] As a consequence, development of new methodologies employing facile, eco-friendly and atom-efficient reactions is considered very important.[5]

Photocatalysis is highly advocated in organic synthesis due to its advantages such as mild operation conditions at room temperature and atmospheric pressure, traceless photons as reagents, and less waste production.[6] Therefore, the synthesis of functionalized indoles and related heterocycles under transition-metal photocatalysis has drawn considerable attention and achieved great successes.[7] In particular, the direct photoconversion of simple structures to more complex indole products is one of the most suitable methods for the preparation of highly functionalized indole derivatives.[8,9] In photochemistry, it has become most common to use high energy-efficient light emitting diodes (LEDs) as quasi-monochromatic light sources for photoreaction test rigs since the wavelength of the maximum peak emission can be selected depending on optical properties of the photocatalyst.[10,11] Notwithstanding that a considerable irradiation time in a batch reactor is often employed to achieve good conversions and get satisfactory isolated yields, ranging from hours to days due to the inhomogeneity of the radiation distribution inside the batch reactor. One of the most promising strategies to circumvent this drawback is the use of micro process technology which benefits from larger surface-to-volume ratio, more efficient mass and heat transfer, lower solvent and reagent consumption, easier scalability and higher productivity.[12] Of special interest is the integration of microreactor technologies and photochemical processes since this can lead to higher selectivity and reduced reaction times due to

[a] *Institute for Micro Process Engineering (IMVT), Karlsruhe Institute of Technology (KIT), Kaiserstraße 12, Karlsruhe, 76131, Germany. E-mail: jun.li@kit.edu*
[b] *Institute of Biological and Chemical Systems (IBCS-FMS), Karlsruhe Institute of Technology (KIT), Kaiserstraße 12, Karlsruhe, 76131, Germany*
[c] *Paul Wurth Chair in Energy Process Engineering, Faculty of Science, Technology and Medicine, University of Luxembourg, Luxembourg*
[d] *Institute of Organic Chemistry (IOC), Karlsruhe Institute of Technology, Kaiserstraße 12, Karlsruhe, 76131, Germany*

† Electronic supplementary information (ESI) available. See DOI: https://doi.org/10.1039/d4re00087k

‡ These authors contributed to the work equally and should be regarded as co-first authors.

the more uniform irradiation and improved mixing. Furthermore, the flexibility of miniaturized LEDs gives them the ability to be perfectly integrated into the flow microreactors, resulting in a powerful set-up for the estimation of reaction kinetics and for scale-up of photoreactions as it allows intrinsic rate constants to be extracted from experimental results both in homogeneous[13,14] and heterogeneous photocatalysis.[15–18] A more detailed review on the determination of photoreaction kinetics in microreactors over the past few years has been summarized by Yan *et al.*,[19] including the types of photoreactions studied, the photocatalysts used, and the microreactor assembly schemes.

Most of the literature known photochemical indole syntheses are performed in batch,[20–23] and the examples for their synthesis under flow conditions are still scarce,[24] while associated kinetic studies have not been reported to the best of our knowledge. Determination of reaction kinetic does not only allow conclusions on possible reaction mechanisms, but also helps to optimize the operating conditions in flow. The approach presented in this paper links macroscopic and microscopic characteristics of photochemical processes.

Recently, a novel photochemical reaction to indole derivatives involving a visible light-induced 1,3-acyl shift was published[25] (Fig. 1). The work presented herein aimed to conduct a kinetic study of this newly found reaction in order to propose and validate a reactor model. The reaction was studied in a capillary microreactor on a flow photocatalytic test bench. Dimensionless numbers affecting mass transport (*Pe*, and Da_I, as well as Da_{II}) were employed to evaluate the influence of operating parameters on the reaction outcome. Furthermore, an intrinsic rate constant independent of the reactor geometry and the incident photon flux was extracted, and key factors influencing reaction optimization and process intensifications could be identified, setting ground for the scale-up in flow photochemistry.

Materials and methods

Chemicals

N-Benzyl-2,2,3,3,4,4,5,5,6,6,7,7,8,8,8-pentadecafluoro-*N*-(2(phenylethynyl)phenyl)octanamide was prepared and purified by the methods that were reported recently.[25] $Ir[dF(CF_3)ppy]_2(dtbpy)(PF_6)$ was obtained from Merck. Anhydrous acetone (≥99.8%), potassium ferrioxalate(III) trihydrate, anhydrous sodium acetate (≥99%), and 1,10-phenanthroline were purchased from VWR. Sulfuric acid solutions (0.05 M and 0.5 M) were prepared by diluting concentrated sulfuric acid (98%) with deionized water (Milli-Q, Merck). All commercially available chemicals were used as received without further purification.

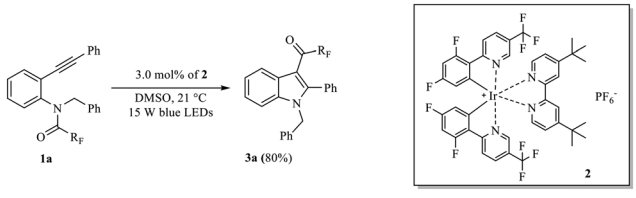

Fig. 1 Recently published photochemical cyclization of F-tagged *o*-alkynylated *N*-alkyl-*N*-acylamides to 3-acylindoles.[25]

Analytical determinations

^1H NMR spectra were recorded on a Bruker Ascend 400 MHz instrument. UV-vis spectra were recorded on the UV-vis spectrophotometer Agilent 8453 in a 10 mm light path optical cuvette.

Photocyclization in the capillary microreactor

Experimental setup. Fig. 2 shows the schematic view of the used continuous-flow system. The capillary microreactor made of PFA tubing (i.d. 0.8 mm, o.d. 1.6 mm) with a total reaction volume of 4 mL was wrapped on a NS 14/23 borosilicate glass tube (o.d. 17 mm) in the shape of a helix (2 mL reaction volume on each tube) and connected with flangeless fittings obtained from IDEX Health & Science (Fig. 3b). The good transparency of PFA materials in the visible light region makes them ideal for simple micro photoreactor fabrication.[17] The rest of the reactor (*e.g.*, infusion tubing) was carefully covered by aluminium foil to prevent undefined extra exposure. The reacting region was fully irradiated by 40 high-power LEDs with the peak emission at λ = 465 nm (adapted from TRU Components, forward current 350 mA, forward voltage 3.4 V, angle 110°) glued on Bosch aluminium profiles (10 profiles with 4 LEDs each, Fig. S1a†). The method implemented here was effective at removing heat even with long-term irradiation (Fig. S1b†). The assembled capillary microreactor was placed at a distance of 2 cm from the LEDs (Fig. 3a). The LEDs were powered by a dimmable 100 W constant current mode LED driver (Meanwell), and the light intensity was modulated by the external variable resistance of the driver depending on the output current provided (Fig. S1c and d†), resulting in a maximum irradiation power of 47.6 W. The strategy adopted here can attenuate the photon flux density entering the

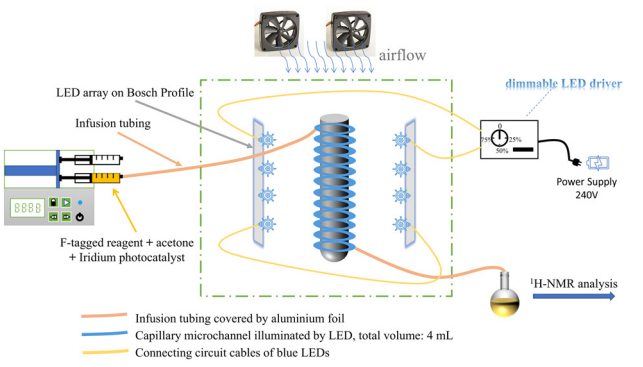

Fig. 2 Schematic diagram of the continuous flow test bench for the photocyclization of the F-tagged aniline derivative to the indole product.

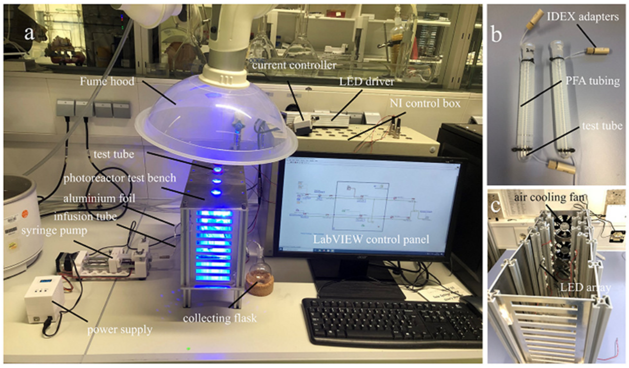

Fig. 3 The experimental setup in this kinetic study. a) Continuous flow system b) PFA capillary microreactor used in the research c) the front view of the photoreactor test bench.

reaction system without changing the spectral irradiance distribution of the LEDs. Two direct current (DC) axial fans were fixed to one side of the test bench (Fig. 3c), connected to NI 9475 digital output channels, and controlled by a LabVIEW program.

Probe reaction and operation conditions. The photoconversion of the F-tagged *o*-alkynylated *N*-alkyl-*N*-acylamide **1a** (25 mM solution in acetone) to the indole product **3a** was performed (Fig. 4), and a moderate catalyst loading of 3 mol% $Ir[dF(CF_3)ppy]_2(dtbpy)(PF_6)$ **2**, shown as the optimum catalyst loading for the batch synthesis, was employed. To be as precise as possible in determining the yield, acetone was used as the solvent since it could easily be evaporated from the reaction mixture compared to DMSO which was used for the corresponding experiment in batch. Experiments in flow were evaluated by varying the flow rate Q (resulting in a mean hydrodynamic residence time ranging from 5 to 180 min) and the incident radiation power P (four intensity levels, 40–100%).

The substrate **1a** (0.1 mmol) and the iridium photocatalyst **2** (3 mol%) were first dissolved in acetone in a flask to obtain 4 mL of a homogeneous solution, which was then transferred to a 10 mL HSW syringe and injected into the assembled photoreactor using a syringe pump. When the syringe was empty, extra 8 mL of fresh acetone were loaded as carrier liquid and mounted on the syringe pump again to continue the infusion process to collect the reaction mixture. Due to the characteristics of laminar flow, the diffusion in the axial direction was negligible. This was backed by a Reynolds number in the range of 1.5 to 52.7 and a Dean number in the range of 0.23 to 8.2, indicating stable laminar flow.[26,27] Therefore, the carrier fluid more or less acted as a piston that pushes the reaction fluid through the photoreactor. The replacement of the syringe took only a few seconds, and the LEDs were switched off once all the mixture had been collected. The solvent from the collected reaction mixture was evaporated, and the crude product was then used for the NMR yield determination.

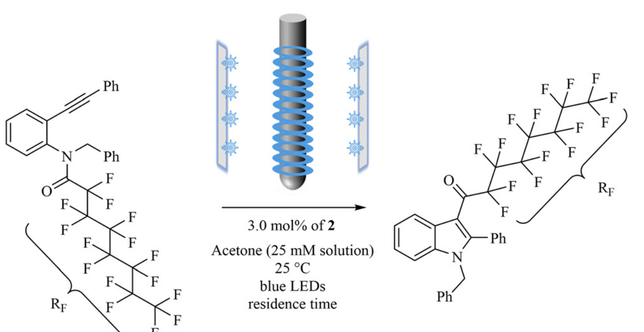

1a 3a

Fig. 4 Visible-light-induced cyclization of F-tagged *o*-alkynylated *N*-alkyl-*N*-acylamide **1a** to indole **3a**.

Modelling of the photocatalytic system

Representation of the photocatalytic reaction rate. The reaction rate in photocatalysis depends, in addition to the photocatalyst and its concentration in the reaction mixture as well as temperature, on the substrate concentration and on the incident light intensity.[28] In general, heat sink should be properly introduced into the photoreactor system as the side effects accompanying peripheral heating in the vicinity of the light source may have an impact on the thermal path of the photoreaction, leading to a possible increase in the proportion of by-products and impaired selectivity.[29] In the presented test bench, the system temperature could be kept close to room temperature (25 ± 3 °C). Therefore, the process could be considered as isothermal. A classical rate expression obeying the plug flow behaviour is described in eqn (1) and (2),

$$r = \frac{-\mathrm{d}C_\mathrm{A}}{\mathrm{d}\tau} = K_\mathrm{app} {C_\mathrm{A}}^n \tag{1}$$

$$K_\mathrm{app} = k_\mathrm{intr} I^\alpha \tag{2}$$

where τ, K_app, C_A, n, k_intr, I and α represent the mean hydrodynamic residence time, the apparent rate constant, the concentration of the substrate **1a**, the reaction order on the substrate concentration, the intrinsic rate constant of the photoreaction, the average incident light intensity, and the constant ranging from 0–1 that depends on the incident light intensity.[30] k_intr could be considered as a constant in this study as the process is isothermal.

The validity of the plug flow model in the rate assumption was examined by the Bodenstein number (Bo), which describes the degree of back mixing by axial diffusion as well as by non-uniform flow velocity.[14,31]

$$\mathrm{Bo} = \frac{\bar{U} \cdot L_\mathrm{cap}}{D_\mathrm{ax}} \tag{3}$$

$$D_\mathrm{ax} = D + \frac{\bar{U}^2 {d_\mathrm{H}}^2}{192D} \tag{4}$$

where $\bar{U}$, L_cap, D_ax, D, and d_H represent the average flow velocity, length of the capillary microreactor, Taylor

dispersion coefficient, the diffusivity of the substrate **1a**, and the hydraulic diameter of the microchannel. The diffusivity of **1a** is not available in the literature. Even though the Wilke–Chang equation is most frequently used one for estimating solute diffusivity in liquid phase systems, the estimated value typically introduces an uncertainty of 10%.[32,33] For the sake of simplification of the evaluation, a reference diffusivity $D = 10^{-9}$ m^2 s^{-1} was adopted for the assessment.[34] The estimated values of Bo varied between 90 to 3240 when the set residence time was in the range of 5 to 180 min. Bo $\gg$ 100 indicates a nearly ideal plug flow behaviour.[35,36] It is clear that not all experimental conditions are applicable in this range, and in some cases the returned Bo values are below 100 but close to its critical value, at least for the shortest residence time experiment of 5 minutes. Therefore, moderate deviations from the plug flow assumption cannot be excluded.

Reactor modelling. The performance of a photoreactor is highly dependent on the reactor geometry and incident light intensity. However, the incident light intensity in a capillary microreactor is difficult to assess with a radiometer and the incident photon flux is often used as an alternative.[37,38] Meanwhile, the apparent rate constant obtained in the eqn (1) and (2) is a macroscopic quantity, which cannot directly reflect the influence of the reactor geometry on the microscopic scale of the reaction. Therefore, a simplified reactor model that takes reactor geometry and incident photon flux into account should be proposed. In addition, reports have shown that the radiative transfer within a similar capillary microreactor can be reduced to a one-dimensional problem and estimated using a constant irradiation profile over the whole cross-section of the capillary.[39–41] Moreover, the effective incident radiation absorption of the photocatalyst can also be evaluated by solving the radiative transfer equation (RTE) with a 1D Monte Carlo method and calibrated with chemical actinometry.[42,43] This strategy provides the opportunity to decouple the radiation transport from reaction kinetics and delineate the interactions with the photocatalyst. Assuming that the light source in this study is monochromatic and the reaction medium is non-emitting and non-scattering, a complete reactor model including the reactor geometry and the incident photon flux can be expressed in eqn (5)–(9).

$$r = k_{\mathrm{intr}} \frac{\left\langle \mathcal{A}_\lambda^{\mathrm{e}} \right\rangle^{\alpha}}{V_{\mathrm{R}}} {C_{\mathrm{A}}}^{n} = k_{\mathrm{intr}} \cdot a_{\mathrm{light}} \cdot {q_{\mathrm{in}}}^{\alpha} \cdot p_{(\Omega)} \cdot {C_{\mathrm{A}}}^{n} \tag{5}$$

$$a_{\mathrm{light}} = \frac{S_{\mathrm{irrad}}}{V_{\mathrm{R}}} \tag{6}$$

$$p_{(\Omega)} = \frac{C_{\mathrm{cat}} E_{\mathrm{cat},\lambda}}{\kappa_{\mathrm{tot},\lambda}} \left[1 - \exp\left(-\kappa_{\mathrm{tot},\lambda} L\right)\right] \tag{7}$$

$$p_{(\Omega)} = \frac{C_{\mathrm{cat}} E_{\mathrm{cat},\lambda}}{\kappa_{\mathrm{tot},\lambda}} \left[1 + \exp\left(-\kappa_{\mathrm{tot},\lambda} L\right)\left(\kappa_{\mathrm{tot},\lambda} - 1\right) + \left(\kappa_{\mathrm{tot},\lambda} L\right)^2 E_{\mathrm{i}}\left(-\kappa_{\mathrm{tot},\lambda} L\right)\right] \tag{8}$$

$$\kappa_{\mathrm{tot},\lambda} = \sum_{i=1}^{n} C_{\mathrm{i}} E_{\mathrm{i},\lambda} \tag{9}$$

k_{intr} presents the intrinsic rate constant which is independent of the reactor geometry and incident photon flux, V_{R} is the reactor volume, $\left\langle \mathcal{A}_\lambda^{\mathrm{e}} \right\rangle$ denotes mean rate of photon absorption of the photocatalyst at specified wavelength λ, α is a constant based on the intensity of the incident photon flux, C_{A} is the cross-sectional concentration of the starting material **1a**, n is the reaction order, a_{light} is the ratio between the irradiated surface S_{irrad} and the reactor volume, V_{R}, q_{in} is the mean incident photon flux density received by the microreactor's wall, and $p_{(\Omega)}$ represents the fraction of light absorbed by the photocatalyst and requires the RTE to be solved by the 1D Monte Carlo method[42] for collimated emission eqn (7) or diffuse emission eqn (8). C_{cat} is the concentration of the photocatalyst **2**, $E_{\mathrm{cat},\lambda}$ represents the Napierian absorption coefficient of the photocatalyst, $\kappa_{\mathrm{tot},\lambda}$ is the summation of the total absorbance of all species in the reaction mixture, L is the light path of the microreactor (i.d. of the used capillary tubing), $E_{\mathrm{i}}(x)$ is the exponential integral function. If the photocatalyst is the only photon absorbing species in the photochemical transformation and homogeneous irradiation is valid, the value of $p_{(\Omega)}$ is fixed and could be considered as a constant. In this scenario, one can deduce that the value of K_{app} is related to the product between a_{light}, ${q_{\mathrm{in}}}^{\alpha}$, and $p_{(\Omega)}$ (eqn (10)).

$$K_{\mathrm{app}} \propto a_{\mathrm{light}} \cdot {q_{\mathrm{in}}}^{\alpha} \cdot p_{(\Omega)} \tag{10}$$

Results and discussion

Incident photon flux determination

To determine the value of the coefficient α in the eqn (2), (5) and (10), and to establish a kinetic model, the photon flux received by the capillary microreactor had to be determined prior to the kinetic evaluation. Chemical actinometry experiments were conducted using potassium ferrioxalate, which is a universal chemical for determining the quantum yield of photoreactions in both batch and flow reactors.[38,44] The mean incident photon flux q_λ (einstein per s) over the capillary microreactor (eqn (S1)†) can be easily derived using the collimated emission (eqn (S2)†) or diffuse emission assumption (eqn (S3)†) based on the conversion of potassium ferrioxalate. In some cases, however, the collimated emission hypothesis is not valid and may lead to overestimation and introduce huge error when the actual emission is closer to Lambertian (*e.g.*, LED).[43] Therefore, the diffuse emission assumption is more appropriate for the system used in this

study. The 1D analytical solutions of eqn (S3)† were calculated with MATLAB R2019a for different light intensities, ranging from 40% to 100% light intensity (see ESI†). Furthermore, to guarantee the accuracy of the derived photon flux in this study, Reinecke's salt was used as a second chemical actinometer,[42,43] and these results were compared to those of potassium ferrioxalate. Table S1† gives the results measured by the two different actinometers, and nearly identical values were obtained, where the unit of "einstein" represents the energy carried by one mole of photons. The calibration values from ferrioxalate were employed for further analysis. For the strongest illumination case (1.15×10^{-5} einstein per s), the incident light intensity in the capillary microreactor was found to be 148.0 W m^{-2} according to the Planck–Einstein relation. The conversion of the unit from einstein per s into W m^{-2} is shown in eqn (11) and (12):

$$E_\lambda = \frac{hc}{\lambda} \tag{11}$$

$$I = \frac{q_\lambda N_A E_\lambda}{S_{irrad}} \tag{12}$$

where h is Planck's constant (6.63×10^{-34} J s), c is the speed of light (3×10^8 m s^{-1}), λ is the maximum emitting wavelength of the used LED (465 nm), and N_A is Avogadro's number (6.02×10^{23}).

The resulting photon flux (148.0 W m^{-2}) is still in the weak absorption region,[30] of which region the light intensity is generally considered below 200.0 to 250.0 W m^{-2}. Therefore, α in the eqn (5) can be set equal to 1.

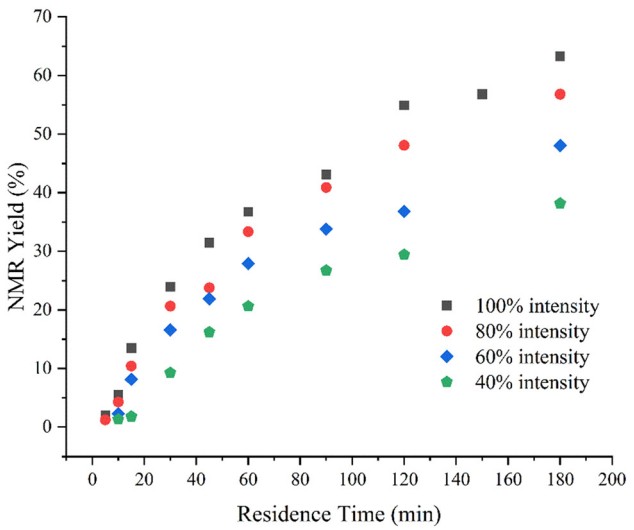

Fig. 5 The NMR yield of the photoreaction under different light intensities and residence times in the capillary microreactor, reaction condition: 25 mM F-tagged acylamide **1a**, 3 mol% Ir[dF(CF$_3$)ppy]$_2$(dtbpy)(PF$_6$) **2** in anhydrous acetone, 465 nm blue LED illumination, the reaction temperature was set at room temperature, LED energy output ranging from 40–100%.

Experimental evaluation of kinetic parameters

The NMR yield (calculated by the ratio of the substrate and product signals in proton spectrum) was employed to extract kinetic parameters by varying the residence time of the reaction mixture and adjusting the incident light intensity in the capillary microreactor.

As shown in Fig. 5, an overview of the experimental results for residence times ranging from 5 to 180 minutes and four levels of light intensity at 465 nm is provided. With an increase in light intensity from 40% to 100%, there is a significant surge in yield with different residence times. When the residence time was 120 minutes, the yield was almost doubled by using 100% intensity instead of 40% light intensity, resulting in conversions of 55% and 29%, respectively. The light intensity effect decreased slightly when the residence time was extended to 180 minutes (63% and 38%, respectively). This is reasonable as the reaction rate drops steeply due to depleted substrate concentration. On the other hand, a lower light intensity results in a smaller local concentration of activated species and reduced number of effective molecular collisions, therefore a lower curvature of the yield profiles under weaker irradiation can be observed. With the yield profiles at hand, the rate constants under different levels of irradiation could be derived. Assuming that the photoreaction was conducted in an isothermal, constant volume plug flow reactor with uniform photon absorption everywhere in the reaction volume, and the reaction obeys simple power-law, the material balance takes the form of eqn (13). By integration, the relationship between concentration and residence time can be easily established and is given in eqn (14)–(16), which stands for zero, first, and neither zero nor first order kinetics assumptions, respectively.

$$\tau = \int_{C_{A0}}^{C_A} \frac{-dC_A}{r} = \int_{C_{A0}}^{C_A} \frac{-dC_A}{K_{app} {C_A}^n} \tag{13}$$

$$C_A = C_{A0} - K_{app}\tau \tag{14}$$

$$C_A = C_{A0} \times \exp(-K_{app}\tau) \tag{15}$$

$$C_A = \left[(n-1)K_{app}\tau + {C_{A0}}^{1-n}\right]^{\frac{1}{1-n}} \tag{16}$$

The value of K_{app} under the strongest irradiation level (100% intensity) was first evaluated from the experimental results by minimizing the residual sum of squares (*RSS*, formulated in eqn (17)) according to the corresponding reaction order assumption. The values of C_A at different residence times and light intensities were backward calculated from the NMR yield shown in Fig. 5.

$$RSS(n, K_{app}) = \sum (C_{A,model} - C_{A,exp})^2 \rightarrow \min \tag{17}$$

The regression of the kinetic parameters (n and K_{app}) was processed with software package MATLAB R2019a, and nonlinear curve fitting was employed with the least-squares

Table 1 Estimated kinetic parameters based on RSS analysis using MATLAB lsqcurfit solver

Entry	Light intensity (%)	Equation assumption	Fitting order (n)	K_{app}	Unit	RSS
1	100	$C_A = C_{A0} - K_{app}\tau$	0	1.08×10^{-4}	M min^{-1}	4.85×10^{-5}
2	100	$C_A = C_{A0} \times \exp(-K_{app}\tau)$	1	0.0065	min^{-1}	1.23×10^{-5}
3	100	$C_A = \left[(n-1)K_{app}\tau + {C_{A0}}^{1-n}\right]^{\frac{1}{1-n}}$	2.0018	0.3799	M^{-1} min^{-1}	2.42×10^{-6}
4	80		2.0021	0.3123		1.17×10^{-6}
5	60		1.9979	0.2096		2.62×10^{-6}
6	40		2.0012	0.1519		2.82×10^{-6}

solver *lsqcurfit*. Table 1 summarizes the obtained estimated parameter values for n, and K_{app}, as well as the residual sum of squares *RSS*. Based on the data, a zero or first order kinetics with regard to the substrate concentration is much less likely than a second order kinetics (entry 1–3 of Table 1). Following the same strategy, apparent rate constants under different irradiation level were obtained as 0.3799, 0.3123, 0.2096, 0.1519 M^{-1} min^{-1} for 100%, 80%, 60% and 40% light intensity (entries 3–6 of Table 1), respectively. Fig. 6a shows the good fit of the experimental data obtained with different light intensities by the second-order kinetics. Moreover, the variation of the substrate concentration with residence time predicted by the proposed reaction kinetic model is shown in Fig. 6b, which is also well matched by the experimental results obtained with different light intensities and residence times, except for very short residence times. The latter may be explained by a departure from the plug flow situation at short residence times as indicated by the calculated value of the *Bo* number dropping below 100 for a residence time of 5 min. For all other residence times, the plug flow model can describe the process adequately. Meanwhile, reactor simulations considering hydrodynamics were also carried out to confirm the credibility of the derived kinetic parameters. A 2D axisymmetric reactor model was used to reproduce the experiments (see Fig. S7†), taking advantage of the symmetrical structure of the capillary tubing. In consistent with the previous assumptions, the process was considered to be homogeneous, therefore the derived apparent rate constants were used as inputs for numerical simulations at different mean hydrodynamic residence times, and the results obtained are displayed in the ESI† (Table S3). The polarity plot (Fig. S8†) indicates the established reaction kinetics could reproduce the process quite well.

Mass transport diagnosis

Several dimensionless numbers are recommended and employed to evaluate the operating conditions in microreactors from a reaction engineering point of view, giving a tutorial guide for people stepping towards flow photochemistry and scale-up studies.[40,41] The Péclet number (*Pe*, ratio of the characteristic time for diffusion time τ_d to the residence time τ) and the Damköhler numbers (Da_I, residence time τ divided by the characteristic reaction time τ_r and Da_{II}, diffusion time τ_d divided by reaction time scale τ_r) were employed as useful dimensionless values to characterize the mass transport within the capillary microreactor. Specifically, the characteristic chemical reaction time τ_r can be estimated from Da_I since its value is equal to the product of the apparent rate constant multiplied by the $n-1$ order of the initial substrate concentration and the residence time τ in a convective

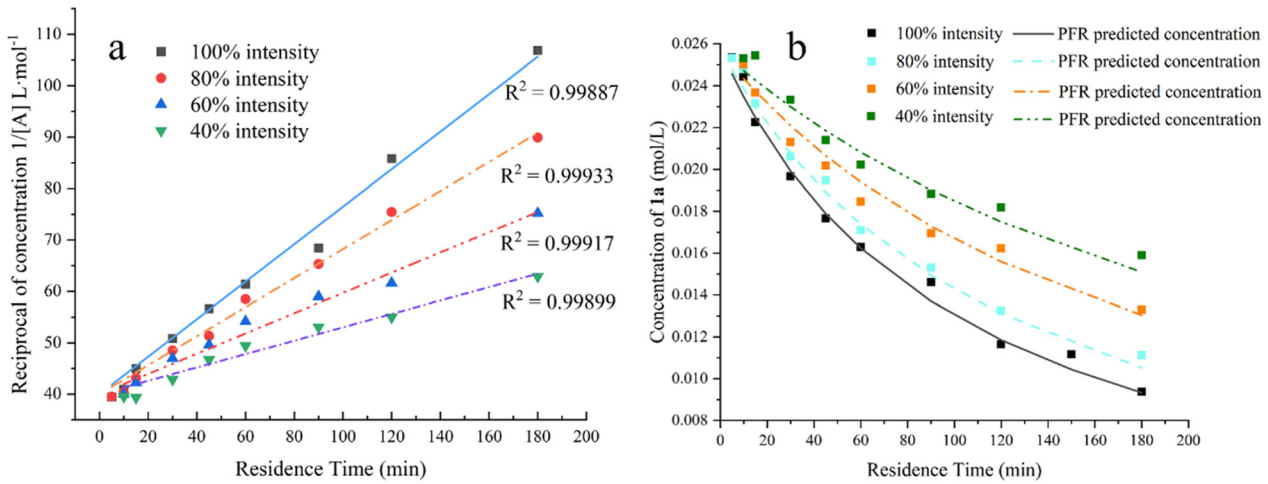

Fig. 6 a) Validation of the second order reaction assumption by plotting the reciprocal of **1a** concentration *versus* residence time. b) Comparison of PFR model predicted and experimental **1a** concentration under different light intensities. 25 mM F-tagged acylamide **1a**, 3 mol% Ir[dF(CF_3)ppy]$_2$(dtbpy)(PF_6) **2** in anhydrous acetone, 465 nm blue LED illumination, the reaction temperature was set at room temperature with the LED energy output ranging from 40–100%.

Table 2 Characteristic time and relative dimensionless numbers in this study

Name	Symbol	Expression	Values
Residence time	τ	$\tau = \frac{V_R}{Q}$	5–180 min
Radial diffusion time	τ_d	$\tau_d = \frac{{d_H}^2}{D}$	10.7 min
Characteristic chemical reaction time	τ_r	$\tau_r = \frac{1}{K_{app}{C_0}^{n-1}}$	263–105 min
Péclet number	*Pe*	$\mathrm{Pe} = \frac{\tau_d}{\tau}$	2.14–0.059
Damköhler I number	Da_I	$\mathrm{Da_I} = \frac{\tau}{\tau_r} = K_{app}{C_0}^{n-1}\tau$	0.048–1.71
Damköhler II number	Da_{II}	$\mathrm{Da_{II}} = \frac{\tau_d}{\tau_r}$	0.10–0.041

flow system. Table 2 lists the values of these calculated dimensionless numbers for the operating conditions covered in this study. For a second-order reaction (n = 2), the value of τ_r is estimated to be 105 min, which corresponds to the case of the highest reaction rate and the minimum value of τ_r in this work. In this context, the estimated value of Da_{II} is always much smaller than 1. As a result, as long as the Péclet number is less than 1 (for cases where the residence time is higher than 10.7 min), the operation conditions always fall in the ideal operating domain where radial concentration gradients can be neglected, and the concentration is rather homogeneous over the cross-section of the capillary at the outlet.[15,40] Conversely, when the Péclet number exceeds 1 (*i.e.*, the case of experimental residence times of 5 or 10 minutes), radial concentration gradients caused by the laminar flow velocity profile cannot be ignored by radial diffusion, resulting in a nonuniform concentration distribution over the cross section along the capillary at the outlet. These findings are consistent with the observation in Fig. 6b that the 5 minute and 10 minute scatters always appear on the upper side of the fitting line for the plug flow reactor model. Fig. 7 presents a diagram associated with the corresponding dimensionless numbers listed in Table 2. The region A stands for the conditions where the reaction mixture is overexposed to the irradiation, and the effect of light attenuation cannot be ignored, while the region B stands for the conditions where both velocity field and reaction kinetics contribute to the generation of concentration gradients within the microreactor. Region C is the recommend operating domain as a homogeneous concentration distribution can be expected at the outlet. Specifically, for the operating regime located in the upper triangle of this region, high conversion can be achieved in the microreactor.[40] Region D represents the situation where a heterogeneous velocity field is the predominant cause of the concentration gradients inside the microchannel. Most of the operating conditions covered in this study fall in region C, only two cases (for a residence time equal to 5 or 10 minutes) appear in region D.

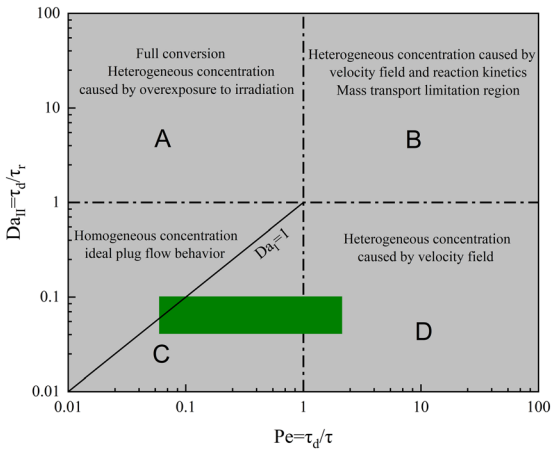

Fig. 7 Damköhler II–Péclet number diagram representing the mass transport phenomena inside the microchannel. The A–D regions represent the different dominant factors affecting mass transport in microreactors. Green rectangle represents the operation conditions implemented in the present work.

Intrinsic rate constant and quantum yield determination

With apparent rate constants K_{app} at hand, the intrinsic rate constant k_{intr} was calculated according to the reactor model shown in eqn (5). The value of the coefficient α was proven to be 1 based on the previous discussion. In addition, Fig. 8a also demonstrates that the apparent rate constant shows good linearity with the mean incident photon flux density, which follows the trend of weak photon absorption. The optical property of the photocatalyst **2** was characterized with an Agilent 8453 UV-vis spectrometer in a 10 mm cuvette and the molar absorption coefficient of the photocatalyst at 465 nm was found to be 209.11 L mol^{-1} cm^{-1} (Fig. S6b†). Assuming the probability density function $p_{(\Omega)}$ of the iridium photocatalyst in the eqn (5) is constant (*i.e.*, homogeneous photocatalysis), the value of $p_{(\Omega)}$ was calculated by MATLAB R2019a and a value of 0.0591 was obtained. In this scenario, the photon absorption of the iridium photocatalyst with the 3 mol% catalyst loading is still weak (less than 6% of the incident photons are absorbed) due to the short light path, although a catalyst loading of a 3 mol% was considered optimal in the batch reactor.[25] The situation does not hold true for the microreactor. Finally, according to eqn (10), by plotting the apparent rate constant against the product of a_{light}, q_{in}, and $p_{(\Omega)}$, the slope of the fitting line indicates the

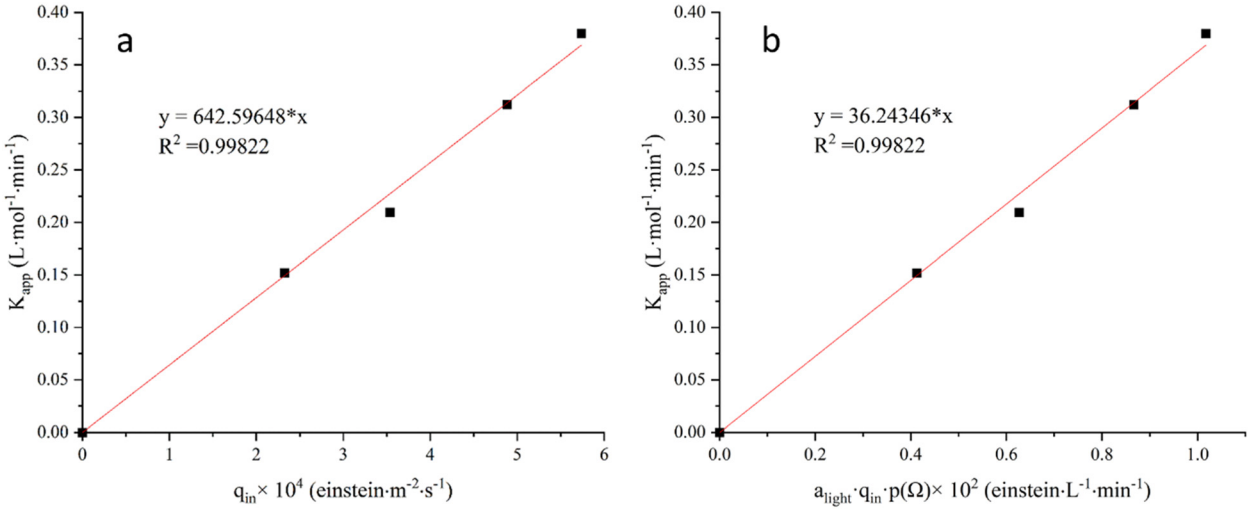

Fig. 8 The linear relationship between (a) apparent rate constant and mean incident photon flux density q_{in} (b) apparent rate constant and the multiply value of a_{light}, q_{in}, and the probability density function $p_{(\Omega)}$ of the iridium photocatalyst at 465 nm.

intrinsic rate constant k_{intr}, giving a value of 36.24 L^2 mol^{-1} per einstein (Fig. 8b). The $p_{(\Omega)}$ value of the iridium photocatalyst was further used to calculate the absorbed incident photon flux by the photocatalytic system to derive the quantum yield of the photoreaction. Table S2† lists the results of the mean incident photon flux for diffuse emission and the mean incident photon flux absorbed by the photocatalyst. With the mean absorbed incident photon flux at hand, the moles of absorbed photons can be deduced. Therefore, the quantum yield of the photoreaction can be derived from eqn (18).

$$\Phi = \frac{\text{moles of produts produced}}{\text{moles of photons absorbed}} \quad (18)$$

Fig. 9a shows the quantum yield profile over the residence time, where the same trend can be observed with different incident photon fluxes in flow experiments: the value increases sharply in the low conversion region and then decreases slowly as the reaction proceeds, which indicates there are two different stages of acceleration and deceleration in this process. For different light intensities, the stronger the intensity used, the smaller quantum yield will get after the same irradiation time. Typically, for homogeneous reactions where only the photocatalysts absorb photons, this value should be a constant. To figure out why this is not the case here, the UV-vis spectra of all species were measured (Fig. 9b). It became clear that the indole product contributes a trivial but noteworthy photon absorption around the wavelength of 465 nm. Therefore, a fraction of photons will be allocated to the product as the reaction proceeds, resulting in reduced photon absorption by the iridium photocatalyst, thereby lowering the reaction rate for elevated conversion. In summary, higher conversions are always accompanied by diminished quantum yields in this photochemical transformation, making

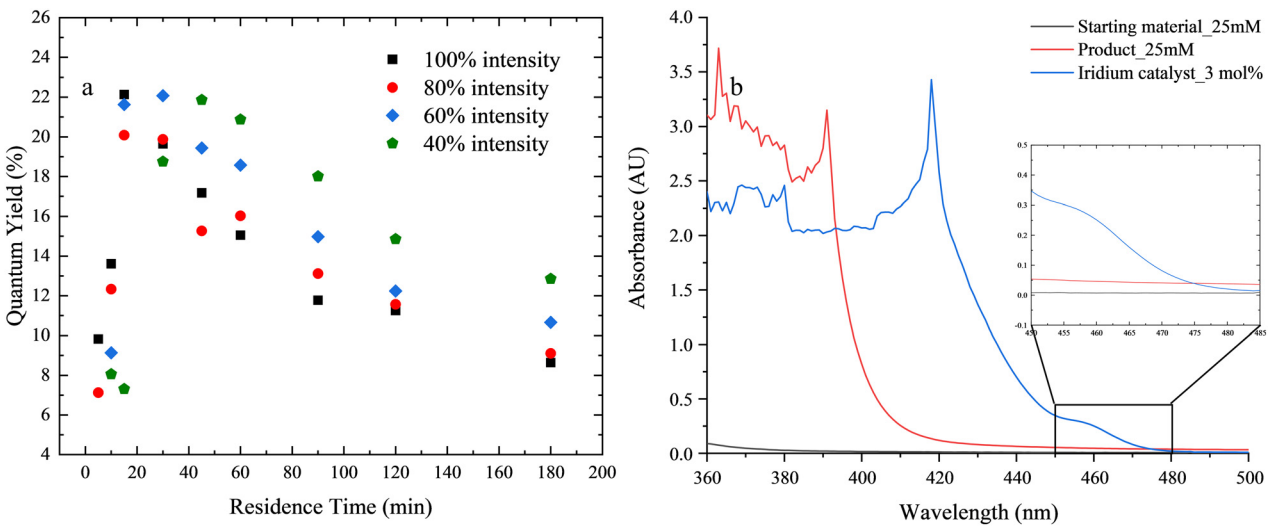

Fig. 9 (a) Plot of quantum yield *versus* residence time at different light intensities under 465 nm LED illumination. (b) UV-vis spectra of all species in the reaction mixture. The inset is the zoom-in view around 450–480 nm.

the photon absorption less effective. Even though the indole product **3a** has been shown to absorb a part of the incoming light, this effect is negligible. Even at complete conversion, the photon absorption of the product is still an order of magnitude smaller than that of the photocatalyst **2**. Therefore, within the range of experimental conditions covered (under 100% light intensity, the conversion is only 63% at a residence time of 180 minutes), the whole process can be considered as homogeneous.

Process intensification in microreactors

The space–time yield (STY) is commonly used to compare the performance of chemical reactors. Its definition is given in eqn (19). For the highest mean hydrodynamic residence time (3 hours) applied in this study, STY values of 5.275 mmol L^{-1} h^{-1}, 4.735 mmol L^{-1} h^{-1}, 4.007 mmol L^{-1} h^{-1} and 3.181 mmol L^{-1} h^{-1} were obtained at light intensities of 100%, 80%, 60%, and 40%, respectively (Fig. 5).

$$\mathrm{STY} = \frac{\text{Desired prodcut quantity}}{\text{Reactor volume·time}}\ \left(\mathrm{mol\ L^{-1}\ h^{-1}}\right) \qquad (19)$$

The photochemical transformation is significantly accelerated when carried out in the capillary microreactor, as a yield of 63% was achieved with a mean hydrodynamic residence time of only 3 hours under strongest irradiation compared to the batch reactor which required 48 hours to get a comparable conversion.[25] In addition, Table 3 summarizes a comparison of photoreaction kinetics study of this work to several available literature studies, and key information with respect to reactor types, reactions, rate expressions, light sources, as well as the maximum STY values are given. It is worth noting that only the rate constants in the rate expressions of entries 2 and 7 take into account both the effects of the reactor geometry and the incident photon flux, whereas the rest of the rate expressions take into account only a part of the effects. Meanwhile, the STY values vary due to the differences in the configuration of the photocatalytic system, the employed photocatalyst loading and the kinetic parameters of the studied photoreactions. Although the STY value of the reaction has been greatly improved compared to the reaction performed under the same conditions in a batch reactor,[25] it still compares unfavourably with other reactors, which could be further improved by strengthening other determining factors.

On the contrary, the calculated fraction of light absorbed $p_{(\Omega)}$ by the iridium photocatalyst is still quite small (0.0591), which results in low photon efficiency. The photon efficiency could be improved by changing some parameters with respect to the reactor geometry or the reaction conditions. Firstly, for the given photoreactor, the concentration of the photocatalyst can be increased, which is the most straightforward way to improve the $p_{(\Omega)}$ value of used photocatalyst. However, blindly increasing the concentration of the photocatalyst is not the economically most feasible approach, since photon saturation conditions in the photoreactor also have to be considered.[30] In addition, an increase of the optical path of the photoreactor would be another option to increase the value of $p_{(\Omega)}$, as its value is proportional to the actual optical path. In addition to increasing the $p_{(\Omega)}$ value of the used photocatalyst, an enhancement of the incident photon flux q_{in} in the microreactor should also be considered, which can be achieved by narrowing the space between the light source and the microchannel or introducing photon reflection. It should be noted that when the light source is very close to the microchannel, it is difficult to ensure that the thermal path of the photoreaction is not activated by peripheral heating caused by the irradiation, which may result in impaired conversion or selectivity.[29] An effective strategy might be to encapsulate the capillary microreactor in a reflective material.[43]

Table 3 A comparison of photochemical reaction kinetics studies in microreactors

Entry	Reactor type	Reaction	Reaction type	Rate expression	Light power	Max. STY (mmol L^{-1} h^{-1})	Ref.
1	Aerosol photoreactor	Singlet oxygen mediated sulfoxidation	Gas–liquid	$r = kC_{\mathrm{SM}}$	36 W lamp	1.6129	Kayahan, *et al.*[18]
2	TiO_2 coated glass planar microreactor	Clofibric acid photodegradation	Liquid–solid	$r = k\frac{A_{\mathrm{cat}}}{V_{\mathrm{R}}}\left(\langle e_{\mathrm{f}}^{\mathrm{a,s}}\rangle A_{\mathrm{cat}}\right)^{0.5}C$	4 × 8 W UV lamps	N.A.	Satuf, *et al.*[15]
3	TiO_2 fixed-bed microreactor	Photocatalytic phenol dissociation	Liquid–solid	$r = \frac{\sum_{j=1}^{J}\left(\pm\eta_j k_j K_j C_j\right)}{1+\sum_{k=1}^{K} K_k C_k} I^n$	N.A.	0.2999	Krivec, *et al.*[16]
4	PFA microcapillary	Photocatalytic aerobic oxidation of thiophenol	Gas–liquid	$r = k_0 q^{0.6}\varphi^{0.21} C_{\mathrm{sub}} {C_{\mathrm{O_2}}}^2$	N.A.	N.A.	Su, *et al.*[17]
5	PFA microcapillary	Photoisomerization of norbornadiene	Homogeneous	$r = K_{\mathrm{f}} C_{\mathrm{NBD}}$	120 W UV-LEDs strip	225.0725	Shen, *et al.*[13]
6	PFA microcapillary	Photooxidation of benzene	Homogeneous	$r = k{C_{\mathrm{benzene}}}^2 C_{\mathrm{DDQ}}$	33 W LEDs	28.20	Shi, *et al.*[14]
7	PFA microcapillary	Photocyclization of F-tagged acylamide	Homogeneous	$r = k_{\mathrm{intr}} a_{\mathrm{light}} q_{\mathrm{in}} p_{(\Omega)} {C_{\mathrm{A}}}^2$	47.6 W LEDs	5.275	This work

Conclusion

In this work, the continuous-flow photocyclization of an F-tagged amide to the indole derivative was performed in a capillary microreactor under 465 nm blue LED illumination. The operating conditions in flow were screened using the optimal catalyst loading reported for batch synthesis and acetone as a solvent. The effects of residence time and light intensity on the reaction yield were determined to acquire data needed for establishing the reaction kinetics. The photon flux calibration experiments confirmed the weak photon absorption conditions in the microreactor, which solidifies the feasibility of extracting the intrinsic rate constant from the proposed photoreactor model. On the basis of Bodenstein number evaluation, the reaction could be proven to follow a second order rate law with respect to the substrate concentration using plug flow assumption, and corresponding apparent rate constants under different light intensities were determined. In addition, different operation conditions implemented in this study were evaluated by the introduction of dimensionless parameters, and the mass transport phenomena in the capillary microreactor were comprehensively analysed. With the proposed simplified photoreactor model, the intrinsic rate constant of this photoreaction was extracted from experimental results. This value is independent of the reactor geometry and the photon flux received by the micro photoreactor. Moreover, the quantum yield of the photoreaction was evaluated and analysed. It exhibits a quadratic function distribution as a function of time with a downward opening, meaning that two stages of acceleration and deceleration in the reaction process, which was proven by the UV-vis spectrum of all the species in the mixture. In other words, photon competition occurred during this reaction as it was shown that the resulting indole product absorbs a fraction of the incoming light. Nevertheless, the system still behaved like a homogeneous photocatalytic process. Finally, general suggestions from an engineering point of view to improve the STY value of the photoreactor are provided. Further investigations should aim at an increase of the optical thickness of the used microchannel or make maximum use of the incident light for the photochemical transformation. Moreover, with the intrinsic rate constant at hand, one can tailor a special photoreactor suitable for this photocyclization process. This way, the results of this study provide a basis for the scale-up of the technology.

Data availability

Data that refer to the herein described experiments were submitted to the repository Chemotion (**https://www.chemotion-repository.net/welcome**). A summary of all experimental data obtained in this study can be gained with the collection DOI as follows:[45] **https://doi.org/10.14272/collection/HMS_2023-10-26**. Reactor simulations were performed in COMSOL Multiphysics (version 6.0). A demo (.mph file) of this work, related to the simulation results shown in the support information, has been submitted to the Zenodo repository.[46] **https://doi.org/10.5281/zenodo.11107170**.

Conflicts of interest

The authors declare that they have no known competing financial interests or personal relationships that could have appeared to influence the work reported in this paper.

Acknowledgements

The authors acknowledge financial support from the DFG (Deutsche Forschungsgemeinschaft) within the Research Unit 2383 ProMiSe, as well as the support of KNMFi (Karlsruhe Nano Micro Facility). The authors acknowledge the support of the German Research Foundation (NFDI4Chem, project number: 441958208) for the infrastructures used in this project. J. L. is grateful to Mrs. Cornelia Schorle and Mr. Conrad Grehl for the help in building up the test bench. J. L. is also grateful to Dr. Paul Kant for the help with the calibration of ferrous anion assays. H. S. T. is grateful to Dr. Patrick Hodapp for the provision and maintenance of syringe pumps used in this study, as well as for his continuous support during this project.

Notes and references

1 N. K. Kaushik, N. Kaushik, P. Attri, N. Kumar, C. H. Kim, A. K. Verma and E. H. Choi, *Molecules*, 2013, **18**, 6620–6662.
2 T. P. Singh and O. M. Singh, *Mini-Rev. Med. Chem.*, 2018, **18**, 9–25.
3 D. F. Taber and P. K. Tirunahari, *Tetrahedron*, 2011, **67**, 7195–7210.
4 M. Platon, R. Amardeil, L. Djakovitch and J. C. Hierso, *Chem. Soc. Rev.*, 2012, **41**, 3929–3968.
5 T. V. Sravanthi and S. L. Manju, *Eur. J. Pharm. Sci.*, 2016, **91**, 1–10.
6 L. Marzo, S. K. Pagire, O. Reiser and B. Konig, *Angew. Chem., Int. Ed.*, 2018, **57**, 10034–10072.
7 A. A. Festa, L. G. Voskressensky and E. V. Van der Eycken, *Chem. Soc. Rev.*, 2019, **48**, 4401–4423.
8 H. J. Kim, D. C. Fabry, S. Mader and M. Rueping, *Org. Chem. Front.*, 2019, **6**, 2319–2323.
9 J. Zoller, D. C. Fabry, M. A. Ronge and M. Rueping, *Angew. Chem., Int. Ed.*, 2014, **53**, 13264–13268.
10 M. Sender and D. Ziegenbalg, *Chem. Ing. Tech.*, 2017, **89**, 1159–1173.
11 C. P. Haas, T. Roider, R. W. Hoffmann and U. Tallarek, *React. Chem. Eng.*, 2019, **4**, 1912–1916.
12 M. Colella, L. Degennaro and R. Luisi, *Molecules*, 2020, **25**, 3242.
13 C. Shen, M. Shang, H. Zhang and Y. Su, *AIChE J.*, 2020, **66**, e16841.
14 X. Q. Shi, S. Liu, C. Duanmu, M. J. Shang, M. Qiu, C. Shen, Y. Yang and Y. H. Su, *Chem. Eng. J.*, 2021, **420**, 129976.
15 M. L. Satuf, J. Macagno, A. Manassero, G. Bernal, P. A. Kler and C. L. A. Berli, *Appl. Catal., B*, 2019, **241**, 8–17.

16 M. Krivec, A. Pohar, B. Likozar and G. Dražić, *AIChE J.*, 2015, **61**, 572–581.
17 Y. H. Su, V. Hessel and T. Noel, *AIChE J.*, 2015, **61**, 2215–2227.
18 E. Kayahan, D. Urbani, P. Dambruoso, A. Massi, L. Braeken, T. V. Gerven and M. Enis Leblebici, *Chem. Eng. J.*, 2021, **408**, 127357.
19 Z. Yan, J. Tian, C. Du, J. Deng and G. Luo, *Chin. J. Chem. Eng.*, 2022, **41**, 49–72.
20 P. Zhang, T. Xiao, S. Xiong, X. Dong and L. Zhou, *Org. Lett.*, 2014, **16**, 3264–3267.
21 Q. Shi, P. Li, X. Zhu and L. Wang, *Green Chem.*, 2016, **18**, 4916–4923.
22 X. Wang, M. Yu, H. Song, Y. Liu and Q. Wang, *Chem. Commun.*, 2022, **58**, 9492–9495.
23 S. Lerch, L.-N. Unkel and M. Brasholz, *Angew. Chem., Int. Ed.*, 2014, **53**, 6558–6562.
24 U. K. Sharma, H. P. L. Gemoets, F. Schroder, T. Noel and E. V. Van der Eycken, *ACS Catal.*, 2017, **7**, 3818–3823.
25 H. Simek Tosino, A. Jung, O. Fuhr, C. Muhle-Goll, N. Jung and S. Bräse, *Eur. J. Org. Chem.*, 2023, **26**, e202201132.
26 P. M. Ligrani, *A study of Dean vortex development and structure in a curved rectangular channel with aspect ratio of 40 at Dean numbers up to 430*, NASA, 1994.
27 M. Mansour, D. Thévenin, K. D. P. Nigam and K. Zähringer, *Chem. Eng. Sci.*, 2019, **201**, 382–385.
28 X. Zhan, C. H. Yan, Y. L. Zhang, G. Rinke, G. Rabsch, M. Klumpp, A. I. Schafer and R. Dittmeyer, *React. Chem. Eng.*, 2020, **5**, 1658–1670.
29 T. D. Svejstrup, A. Chatterjee, D. Schekin, T. Wagner, J. Zach, M. J. Johansson, G. Bergonzini and B. Konig, *ChemPhotoChem*, 2021, **5**, 808–814.
30 L. Buglioni, F. Raymenants, A. Slattery, S. D. A. Zondag and T. Noël, *Chem. Rev.*, 2022, **122**, 2752–2906.
31 A. Delparish, A. Uslu, Y. Cao, T. de Groot, J. van der Schaaf, T. Noël and M. Fernanda Neira d'Angelo, *Chem. Eng. J.*, 2022, **438**, 135393.
32 K. Miyabe and R. Isogai, *J. Chromatogr. A*, 2011, **1218**, 6639–6645.
33 R. H. Perry, D. W. Green and J. O. Maloney, *Perry's chemical engineers' handbook*, 7th edn, 1997.
34 Y. Cao, C. Soares, N. Padoin and T. Noël, *Chem. Eng. J.*, 2021, **406**, 126811.
35 M. T. Kreutzer, J. J. W. Bakker, F. Kapteijn, J. A. Moulijn and P. J. T. Verheijen, *Ind. Eng. Chem. Res.*, 2005, **44**, 4898–4913.
36 K. D. Nagy, B. Shen, T. F. Jamison and K. F. Jensen, *Org. Process Res. Dev.*, 2012, **16**, 976–981.
37 B. Wriedt, D. Kowalczyk and D. Ziegenbalg, *ChemPhotoChem*, 2018, **2**, 913–921.
38 T. Aillet, K. Loubiere, O. Dechy-Cabaret and L. Prat, *Int. J. Chem. React. Eng.*, 2014, **12**, 257–269.
39 R. P. M. Moreira and G. Li Puma, *Chem. Eng. J.*, 2021, **415**, 128833.
40 T. Aillet, K. Loubière, L. Prat and O. Dechy-Cabaret, *AIChE J.*, 2015, **61**, 1284–1299.
41 K. Loubiere, M. Oelgemoller, T. Aillet, O. Dechy-Cabaret and L. Prat, *Chem. Eng. Process.*, 2016, **104**, 120–132.
42 V. Rochatte, G. Dahi, A. Eskandari, J. Dauchet, F. Gros, M. Roudet and J. F. Cornet, *Chem. Eng. J.*, 2017, **308**, 940–953.
43 R. Radjagobalou, V. D. D. Freitas, J. F. Blanco, F. Gros, J. Dauchet, J. F. Cornet and K. Loubiere, *J. Flow Chem.*, 2021, **11**, 357–367.
44 C. G. Hatchard and C. A. Parker, *Proc. R. Soc. London, Ser. A*, 1956, **235**, 518–536.
45 H. Šimek Tosino, *Chemotion Repository*, 2024, DOI: **10.14272/collection/HMS_2023-10-26**.
46 J. Li, 2D axisymmetric simulation of photocyclization reactions (probe reaction) in a capillary microreactor_support information_COMSOL Demo, DOI: **10.5281/zenodo.11107170**.